PCCP

Accepted Manuscript

ROYAL SOCIETY OF CHEMISTRY

www.rsc.org/pccp

Physical Chemistry Chemical Physics

ARTICLE

Theory for spiralling ions for 2D FT-ICR and comparison with precessing magnetization vectors in 2D NMR

Akansha Ashvani Sehgal[a,b,c], Philippe Pelupessy[a,b,c], Christian Rolando[d,e,f] and Geoffrey Bodenhausen*[a,b,c]

Two-dimensional (2D) Fourier transform ion cyclotron resonance (FT-ICR) offers an approach to mass spectrometry (MS) that pursuits similar objectives as MS/MS experiments. While the latter must focus on one ion species at a time, 2D FT ICR can examine all possible correlations due to ion fragmentation in a single experiment: correlations between precursors, charged and neutral fragments. We revisited the original 2D FT-ICR experiment that has hitherto fallen short of stimulating significant analytical applications, probably because it is technically demanding. These shortcomings can now be overcome by improved FT-ICR instrumentation and computer hard- and software. We seek to achieve a better understanding of the intricacies of the behavior of ions during a basic two-dimensional ICR sequence comprising three simple monochromatic pulses. Through simulations based on Lorentzian equations, we have mapped the ion trajectories for different pulse durations and phases.

Key words: Precursor ions, fragment ions, off-centered trajectories

Abbreviations: 2D FT-ICR-MS: Two-Dimensional Fourier Transformation Ion Cyclotron Resonance Mass Spectroscopy, NMR: Nuclear Magnetic Resonance

Introduction

Two-dimensional nuclear magnetic resonance (NMR) has inspired the development of 2D techniques in several more or less related fields like infrared (IR) spectroscopy,[1] electron spin resonance (ESR),[2] ion cyclotron resonance (ICR),[3] electron spectroscopy (ES),[4] and femtosecond optical spectroscopy.[5] So far, most of these 2D techniques have not achieved an impact comparable to the revolution that occurred in NMR. Two-dimensional Fourier transform ion cyclotron resonance mass spectroscopy (2D FT-ICR-MS) was initiated nearly 30 years ago through a joint effort of MS and NMR groups.[3] This work was inspired by two-dimensional exchange spectroscopy (2D EXSY), also known as nuclear Overhauser effect spectroscopy (NOESY), which is widely used to either obtain information on chemical reactions that involve sites which differ in chemical shifts, or on the migration of magnetization due to cross-relaxation.[6] As the inspiration for 2D ICR comes from 2D NMR, we shall develop simple models to explain the behaviour of ions in ICR in analogy to the magnetization vectors used in NMR, in view of exploring their similarities and differences.

Both EXSY and NOESY NMR experiments can be understood in terms of classical magnetization vectors that obey Bloch's equations. These vectors follow trajectories that are confined to a sphere with unit radius. Relaxation causes the vectors ultimately to return to the North Pole of Bloch's sphere, which therefore acts as an 'attractor'. The curvature of this sphere is responsible for many non-linear effects in NMR, which are pronounced when using pulses with large nutation angles, but can be neglected if the perturbations are weak. The trajectories of ions in 2D ICR also exhibit a linear response if the perturbations are weak, but these trajectories are not necessarily confined to the centre of the ICR cell. As a result, concepts such as phase-cycles cannot be readily transferred from NMR to ICR.

[a]*École Normale Supérieure-PSL Research University, Département de Chimie, 24, rue Lhomond, 75005 Paris, France.*
[b]*Sorbonne Universités, UPMC Univ Paris 06, LBM, 4, place Jussieu, 75005 Paris, France.*
[c]*CNRS, UMR 7203 LBM, 75005 Paris, France.*
[d]*Univ. Lille, CNRS, USR 3290, MSAP, Miniaturisation pour la Synthèse l'Analyse et la Protéomique, 59 000 Lille, France.*
[e]*Univ. Lille, CNRS, FR 3688, FRABIO, Biochimie Structurale & Fonctionnelle des Assemblages Biomoléculaires,59 000 Lille, France.*
[f]*Univ. Lille, CNRS, FR 2638, Institut Eugène-Michel Chevreul, 59 000 Lille, France.*

**Geoffrey.Bodenhausen@ens.fr*

The unparalleled success of 2D NMR has been a source of inspiration for 2D ICR, but also a source of some conceptual misunderstandings. There are indeed close similarities between 2D ICR and 2D EXSY. In either case, the magnetic field leads to circular motions: in NMR the sense of precession of the magnetic moments is determined by the sign of the gyromagnetic ratio, while in ICR it is the charge of the ions that determines the sense of cyclotron motions.[7,8] On the one hand, 2D EXSY and 2D NOESY allow one to correlate pairs of chemical shifts that are characteristic of the environments of nuclei before and after a chemical reaction or cross-relaxation process. On the other hand, 2D ICR allows one to correlate pairs of cyclotron frequencies that are characteristic of precursor and fragment ions before and after a modification of their mass-to-charge ratio due to losses of neutral fragments, protonation, etc. These modifications can be induced by collisions with neutral molecules or by irradiation with infrared or electron beams.

In its most basic form, two-dimensional exchange spectroscopy (2D EXSY), uses a sequence comprising three pulses: $\beta - t_1 - \beta' - \tau_m - \beta'' - t_2$, as shown in Figure 1.The interval t_1 is known as the evolution time, τ_m the mixing interval, and t_2 the detection period. The amplitude of an *rf* pulse can expressed in terms of an angular frequency, $\omega_1 = -\gamma B_1$, and a 'nutation angle' or 'flip angle' given by the pulse area, $\beta = \omega_1 \tau_p = -\gamma B_1 \tau_p$. Thus the three *rf* pulses are characterized by $\beta = \omega_1 \tau_p$, $\beta' = \omega_1' \tau_p'$ and $\beta'' = \omega_1'' \tau_p''$. For ICR, the three-pulse sequence can be denoted as $P_1 - t_1 - P_2 - \tau_m - P_3 - t_2$. The three pulses can be characterized by the energy they confer to the ions through acceleration (or withdraw through their deceleration). This energy is determined by the product of the pulse durations T_1, T_2 and T_3 and their amplitudes E_1, E_2 and E_3. In ICR, there is no universally accepted expression for the area of a pulse $A_i = T_i E_i$, i.e., for the product of its duration T_i and its amplitude E_i.

In NMR, the basic sequence mentioned above can be traced back to early work on 'stimulated echoes'.[9] Part of the magnetization, said to be 'transverse', precesses in a plane perpendicular to the applied magnetic field B_0, both in the evolution interval t_1 and in the detection interval t_2. On the other hand, only 'longitudinal' magnetization that is parallel to the applied magnetic field B_0 needs to be considered in the mixing interval τ_m. In ICR, if we neglect so-called 'magnetron motions', the motion of the ions is limited to a plane perpendicular to the applied magnetic field B_0, so that one cannot speak of any longitudinal component. In NMR, the frequency range, $\Delta\omega_0$ is usually of the order of a few tens or hundreds of parts per million (ppm), centred on the Larmor frequency of the nuclei under investigation. All three *rf* pulses can have the same monochromatic carrier frequency, provided their *rf* amplitude is sufficient to cover the required frequency range, i.e., provided $\omega_1 = -\gamma B_1 > \Delta\omega_0$. By contrast, ICR frequencies can range from a few kHz to many MHz. To cover such large bandwidths, one usually has to employ frequency-swept 'chirp' pulses.

In their most common forms, 2D EXSY or NOESY use three equal nutation angles $\beta = \beta' = \beta'' = \pi/2$. By analogy, the original 2D ICR experiments used three pulses with the same durations $T_1 = T_2 = T_3$, the same amplitudes $E_1 = E_2 = E_3$ and hence the same 'pulse areas' $A_i = T_i E_i$. If 2D EXSY experiments are performed using three pulses with identical flip angles, $\beta = \beta' = \beta'' = \pi/2$, the fate of the magnetization can be readily described. The first pulse converts the longitudinal magnetization M_z^k of a site *k* into a transverse component M_x^k, the second pulse β' has the opposite effect and generates a t_1-dependent longitudinal component $M_z^k(t_1)$, while the remaining transverse components M_x^k and M_y^k can be suppressed by applying pulsed field gradients (PFGs) or by phase cycling (*vide infra*). The longitudinal component can be partly transferred from a site *k* to a site *l*, i.e., from $M_z^k(t_1)$ to $M_z^l(t_1)$, through exchange or cross-relaxation, and finally reconverted by the third pulse β'' from M_z^l into M_x^l. This transverse term induces a signal in the detection interval t_2. Unlike many other 2D NMR experiments that involve a transfer of coherence, and therefore require a quantum-mechanical treatment, most applications of 2D EXSY and NOESY can be discussed purely in classical terms (except for some artifacts known as '*J*-peaks' that are due to the unwitting excitation of zero-quantum coherences). In NMR, this means that the Bloch equations are sufficient, without resorting to density operators, so that each spin I^k (k = 1, 2 … K) can be associated with a classical magnetization vector $\boldsymbol{M}^k = (M_x^k, M_y^k, M_z^k)$.

Relaxation can be treated in simple phenomenological terms. The transverse components M_x^k and M_y^k decay with a time constant T_2, while the longitudinal component M_z^k returns to its equilibrium with a time constant T_1. If relaxation can be neglected, the trajectory of a vector $\boldsymbol{M}^k$ in the course of multiple-pulse experiments can be described on the surface of what is commonly referred to as Bloch's sphere. Note that the curvature of this sphere is responsible of the non-linearity of the response of the magnetization in NMR. As we shall see below, there is no analogy in ICR for such non-linear effects.

Although this does not appear to be common practice, one can modify 2D EXSY NMR by using pulses with small flip angles $\beta' = \beta'' << 90^o$, say 15^o, while the first pulse may remain $\beta = 90^o$ without loss of generality. This can be used to map longitudinal relaxation pathways in systems with scalar-coupled spins or to obtain z-filtered COSY spectra.[10–13] Although 2D EXSY with small flip angles remains rather confidential in NMR, it offers straightforward analogies with 2D ICR. Indeed, by using only small nutation angles, the excursions of the vectors $\boldsymbol{M}^k$ are limited to the vicinity of the North Pole of Bloch's sphere. The precession of a magnetization vector leads to a circular trajectory around the North Pole in a plane that is parallel to the equatorial plane. If one focuses attention on this plane and neglects the curvature of the sphere, the non-linearity of the response can be ignored, so that NMR becomes analogous to ICR in this linear regime.

While this analogy has lead to the realization that 2D EXSY could simply be 'carried over' from NMR to ICR, it has also given rise to some misunderstandings. In NMR, regardless whether the description is limited to the polar region of Bloch's sphere or not, the North Pole acts as an 'attractor'. Deviations from the North Pole only arise if there are non-vanishing transverse magnetization components. Not only do these components decay through transverse T_2 relaxation, but they can be suppressed either by applying pulsed field gradients (PFG), i.e., by deliberately degrading the homogeneity of the field B_0 during a brief interval, or by phase-cycling. A phase-cycle consists in combining several experiments with the same sequence of pulses and the same intervals, but where the phase ϕ_i of the i^{th} pulse in the sequence is incremented from one scan to the next, i.e., $\phi_i = \phi_i^0 + k\Delta\phi_i$ for the k^{th} scan in a series of scans with $k_i = 0, 1, 2, \ldots, (K_i\text{-}1)$ complementary experiments that are identical except for the phases of the pulses that are incremented in steps $\Delta\phi_i = 2\pi/K_i$. In the common case where $K_i = 2$ and hence $\Delta\phi_i = \pi$, a phase-cycle boils down to a simple two-step phase alternation. Regardless of the nutation angles β and β', such a two-step cycle can be applied either to the first or second pulse in 2D EXSY, combined with alternating addition and subtraction of the resulting signals (which for $K_{rec} = K_i = 2$ can be achieved by alternating the receiver phase $\phi_{rec} = k\Delta\phi_{rec}$ with $k = 0$, 1 and $\Delta\phi_{rec} = 2\pi/K_{rec} = \pi$). This leads to the cancellation of transverse magnetization components in the mixing interval τ_m. Such methods can be understood in terms of 'coherence transfer pathways', where transverse magnetization components correspond to coherences of order $p = \pm 1$, while longitudinal magnetization components have order $p = 0$.[14] Unfortunately, it is not possible to extend these concepts to ICR, where one cannot make a distinction between longitudinal and transverse components. As a result, the ideas underlying phase-cycles cannot be transferred from NMR to ICR.

As mentioned above, the excitation of the magnetization in NMR only remains in the linear regime if the nutation angles are small so that $\sin(\beta) \approx \beta$. This means that the magnetization remains confined to the vicinity of the North Pole of the Bloch sphere. In ICR, the response to excitation is always linear, regardless of the areas $A_i = T_i E_i$ of the pulses, as long as the ions are not ejected from the cell. If we neglect 'magnetron motions', the trajectories of the ions are limited to a plane perpendicular to the applied magnetic field B_0. However, as we shall show below, the trajectories of ions in 2D ICR are not necessarily centred in the middle of the ICR cell.

In the now widely accepted parlance of 2D NMR, the evolution interval $t_1 = n_1\Delta t_1$ is incremented in N_1 steps with $n_1 = 0, 1, 2, \ldots, (N_1\text{-}1)$, while the increment Δt_1 determines the spectral width $\Delta\nu_1 = 1/\Delta t_1$ in the F_1 domain, also known as ν_1 or ω_1 domain. The maximum duration $t_1^{max} = (N_1\text{-}1)\Delta t_1$ determines the digital resolution $\delta\nu_1 = 1/t_1^{max} = \Delta\nu_1/(N_1\text{-}1)$ in the F_1 domain. Likewise, the signal is observed in the detection interval t_2 by taking N_2 samples at intervals Δt_2 that determine the spectral width $\Delta\nu_2 = 1/\Delta t_2$ in the F_2 domain, also known as ν_2 or ω_2 domain. The duration $t_2^{max} = (N_2\text{-}1)\Delta t_2$ determines the

digital resolution $\delta\nu_2 = 1/t_2^{max} = \Delta\nu_2/(N_2\text{-}1)$ in this domain. The same principles apply to 2D FT-ICR spectra. A 2D spectrum can be represented by a contour plot of intensities as a function of two frequencies F_1 and F_2 (also known as ν_1 and ν_2 or ω_1 and ω_2), which are obtained by Fourier transformation of the signals recorded as a function of two time variables t_1 and t_2. The position of each peak is specified by two frequency co-ordinates. By convention, most 2D NMR spectra are plotted so that ω_1, which represents the evolution in the 'indirect' t_1 dimension, appears along the vertical axis, while the 'direct' dimension ω_2 is usually plotted is along the horizontal axis. In ICR, it has become fashionable to speak of 'parent' and 'fragment' dimensions rather than 'vertical' (F_1) and 'horizontal' (F_2) dimensions. A 2D FT-ICR spectrum allows one to map arbitrary correlations between precursor and fragment ions without any a priori information about the samples.

The general scheme for obtaining a 2D FT-ICR spectrum is shown in Figure 2a. The evolution interval t_1 is sandwiched between a first 'excitation' pulse P_1 and a second 'encoding' pulse P_2. The sequence, P_1-t_1-P_2, is collectively referred as the 'encoding sequence'. In an ICR cell, we wish to monitor the conversion of a precursor ion I^k into a fragment ion I^l during the fragmentation interval τ_m, which plays a similar role as the mixing time τ_m in NMR. The fragmentation may be induced by an electron beam, for example by electron capture dissociation (ECD),[15] by electron detachment dissociation (EDD),[16] by electron-induced dissociation (EID),[17] or by electron transfer dissociation (ETD),[18] by infrared light in infrared multiphoton dissociation (IRMPD).[19] Alternatively, ion fragmentation may be brought about by blackbody infrared radiative dissociation (BIRD)[20] or by collisions with neutral molecules in collision-induced dissociation (CID).[21] After the fragmentation interval τ_m, a third 'monitoring' or 'detection' pulse P_3 is applied, and the signals are recorded during the detection period t_2.

The evolution interval t_1 is incremented stepwise and the signals are recorded as a function of t_2 for each value of t_1. After 2D Fourier transformation, one obtains a 2D spectrum as shown schematically in Figure 2b. In ICR, the conversion of a fraction f_{kl} of precursor ions I^k into fragment ions I^l leads to a cross-peak at coordinates ($\omega_1 = \Omega^k$, $\omega_2 = \Omega^l$), with an amplitude proportional to the fraction f_{kl}. Fragmentation leads to a change in mass from m_k to m_l or to a change in charge from q_k to q_l, and hence to a jump in the ICR frequency from a 'parent frequency' $\omega_1 = \Omega^k$ that is proportional to q_k/m_k to a 'daughter frequency' $\omega_2 = \Omega^l$ that is proportional to q_l/m_l. Note that one can have $\Omega^k < \Omega^l$ when ions break up into smaller fragments or acquire a greater charge, and $\Omega^k > \Omega^l$, when ions form larger adducts or lose part of their charge. Such frequency jumps can be readily characterized by 2D ICR.

Frequency-swept 'chirp' pulses are usually applied to excite ions in Penning traps of commercial ICR instruments.[22–24] In our ICR instrument (which is quite different from NMR instruments in this respect), chirp *rf* pulses sweep through a relevant range of frequencies from an initial frequency ω_i to a final frequency ω_f in N discrete steps $\Delta\omega$ of duration ΔT, so that the total pulse duration is $T = N\Delta T$. Usually it can be assumed that the k^{th} ion is only affected by the *rf* irradiation in the k^{th} interval and the frequencies of the adjacent steps are too far off-resonance to influence the motion of the k^{th} ion. The actual evolution interval t_1 between the two pulses of the encoding sequence is therefore equal to the duration between the end of the k^{th} block of the first 'excitation' pulse and the start of the k^{th} block of the second 'encoding' pulse, as shown in Figure 3. Thus the interactions of ions with chirp *rf* pulses can be described as if one used only simple monochromatic pulses. We shall therefore describe the behaviour of a single ion excited by a sequence of monochromatic pulses, and we shall neglect the effects of ion-ion interactions. Although 2D FT-ICR has the potential to become a useful method for chemical analysis, only few studies have been published so far, such as the paper by Guan and Jones on the theory of 2D FT-ICR.[25] Despite its elegant description of the ion trajectories, the assumption that the *rf* pulses should be long turned out to be detrimental to sensitivity. In recent work from our laboratory,[26] we have shown that 2D ICR spectra obtained with shorter pulse durations have higher signal-to-noise ratios. Such spectra are less cluttered by harmonics so that their interpretation is facilitated without requiring sophisticated 'de-noising' algorithms.[26,27] Herein, we describe the behaviour of ions when the pulses are short.

Theory

Equations of motion for 2D FT-ICR

In an ICR cell, the ions are subjected to a static magnetic field $\overrightarrow{B_0} = (0, 0, B)$ and to a perpendicular electric field $\overrightarrow{E(t)} = (E_x, 0, 0)$. A precursor ion I^k of mass m_k and charge q_k moves on a circular trajectory in a plane perpendicular to the magnetic field. The motion is determined by the Lorentz equation:

$$m_k \frac{d\overrightarrow{v_k}}{dt} = q_k\vec{E} + q_k(\overrightarrow{v_k} \times \vec{B}) \quad (1)$$

If there is no applied electric field, the cyclotron frequency is:

$$\omega_k = (q_k B)/m_k \quad (2)$$

We shall neglect 'trapping' motions along the z-axis, and assume that the magnetic field is homogeneous across the ICR cell. We shall also neglect ion-ion Coulomb repulsions, although Chen and Comisarow have shown that these interactions lead to a dispersion of ion clouds, thus affecting the phases of the ions and the radii of their trajectories.[28]

The electric field in ICR is usually applied in the form of frequency-swept 'chirped' radio-frequency (*rf*) pulses. To simplify the discussion, we shall discuss monochromatic *rf* pulses which are 'on resonance', i.e., with a carrier frequency ω_k that matches the cyclotron motion of the parent ion I^k during the first two pulses of lengths $T_1 = T_2 = T$ with amplitudes $E_1 = E_2 = E$ (intervals 0-1 and 2-3 in Figure 2):

$$E_x = E\sin(\omega_k t) \quad (3)$$

The components v_{kx} and v_{ky} of the parent ion I^k can easily be determined by substituting Eq. 2 to solve Eq.1:

$$\frac{dv_{kx}}{dt} = \frac{q_k E_x}{m_k} + \omega_k v_{ky} \quad (4a)$$

$$\frac{dv_{ky}}{dt} = -\omega_k v_{kx} \quad (4b)$$

Solving Eqs.4a and 4b, we get:

$$v_{kx} = v_{kx0}\cos(\omega_k t) + v_{ky0}\sin(\omega_k t) + \frac{Eq_k t\sin(\omega_k t)}{2m_k} \quad (5a)$$

$$v_{ky} = v_{ky0}\cos(\omega_k t) - v_{kx0}\sin(\omega_k t) + \frac{Eq_k t\cos(\omega_k t)}{2m_k} - \frac{Eq_k\sin(\omega_k t)}{2m_k\omega_k} \quad (5b)$$

In our 2D FT-ICR experiments, we used 'chirp' pulses comprising *N* discrete steps with a duration Δ*T* on the order of a few µs. In such cases, the trajectories of the ions during Δ*T* fall short of completing a full orbit along an Archimedes spiral. Therefore, none of the terms of the Eq. 5 can be neglected. In the following sections, analytical solutions are obtained for the velocity components and the position coordinates of an ion at the end of the second pulse, i.e., at the beginning of the fragmentation interval.

a) Excitation pulse

At the end of the first pulse ($t = T_1$ in the scheme of Figure 2), the velocity of the ion is obtained by solving Eq. 5 for the initial condition where $v_{kx0} = v_{ky0} = 0$. We assume that all ions are initially located in the centre of the ICR cell. The corresponding x and y coordinates with respect to the centre of the ICR cell are obtained by integrating their respective velocity components:

$$v_{kx1} = \frac{Eq_k T sin(\omega_k T)}{2m_k} \quad (6a)$$

$$x_{k1} = \frac{Eq_k\{sin(\omega_k T) - \omega_k T cos(\omega_k T)\}}{2m_k\omega_k^2} \quad (6b)$$

$$v_{ky1} = \frac{Eq_k T cos(\omega_k T)}{2m_k} - \frac{Eq_k sin(\omega_k T)}{2m_k\omega_k} \quad (7a)$$

$$y_{k1} = \frac{Eq_k\{2cos(\omega_k T) + \omega_k T sin(\omega_k T) - 2\}}{2m_k\omega_k^2} \quad (7b)$$

b) Evolution interval

During the evolution interval t_1, the electric field is switched off ($E_x = 0$) so that only the phases evolve:

$$v_{kx2} = \frac{Eq_k}{4m_k\omega_k}\{\cos[\omega_k(T + t_1)] - \cos[\omega_k(T - t_1)] + 2\omega_k T sin[\omega_k(T + t_1)]\} \quad (8a)$$

$$x_{k2} = \frac{Eq_k}{2m_k\omega_k^2}\{\cos(\omega_k t_1)\sin(\omega_k T) - \omega_k T cos[\omega_k(T + t_1)]\} \quad (8b)$$

$$v_{ky2} = \frac{Eq_k}{2m_k\omega_k}\{\omega_k T\cos(\omega_k T)\cos(\omega_k t_1)\,\omega_k(T+t_1) - \sin(\omega_k \mathrm{T})[\cos(\omega_k t_1) + \omega_k T sin(\omega_k t_1)]\} \quad (9a)$$

$$y_{k2} = \frac{Eq_k}{4m_k\omega_k^2}\{cos[\omega_k(T+t_1)] - cos[\omega_k(T-t_1)] + 2\omega_k T sin[\omega_k(T+t_1)] + 4\cos(\omega_k T) - 4\} \quad (9b)$$

c) Second pulse

The trajectories can be calculated in analogy to the first pulse, using initial velocities that are equal to the final velocities of Eqs. 8a and 9a. The two first pulses that bracket the evolution time t_1 and together make up the 'encoding sequence', are chosen to be exactly similar, with equal pulse durations, electric field amplitudes, and areas ($T_1 = T_2 = T$, $E_1 = E_2 = E$, $A_1 = A_2 = A$). Inserting these values into Eq.5, we obtain at the end of the second pulse (which is also the beginning of the fragmentation interval τ_m):

$$v_{kx3} = \frac{Eq_k}{4m_k\omega_k}\{\cos[\omega_k(2T+t_1)] - \cos(\omega_k t_1) + 2\omega_k T\{\sin(\omega_k T) + sin[\omega_k(2T+t_1)]\}\} \quad (10a)$$

$$x_{k3} = \frac{Eq_k}{4m_k\omega_k^2}\{2\sin(\omega_k T) - \sin(\omega_k t_1) + \sin[\omega_k(2T+t_1)] - 2\omega_k T\{\cos[\omega_k(2T+t_1)] + \cos(\omega_k T)\}\} \quad (10b)$$

$$v_{ky3} = \frac{Eq_k}{4m_k\omega_k}\{\sin(\omega_k t_1) - 2\sin(\omega_k T) - \sin[\omega_k(2T+t_1)] + 2\omega_k T\{\cos(\omega_k T) + \cos[\omega_k(2T+t_1)]\}\} \quad (11a)$$

$$y_{k3} = \frac{Eq_k}{4m_k\omega_k^2}\{2\omega_k T\{\sin[\omega_k(2T+t_1)] + \sin(\omega_k T)\} + \cos[\omega_k(2T+t_1)] - \cos(\omega_k t_1) + 8\cos(\omega_k T) - 8\} \quad (11b)$$

At the beginning of the fragmentation interval τ_m, the position of an ion with respect to the centre of the cell is given by:

$$|\vec{R}| = \left(x_{k3}^2(T,t_1) + y_{k3}^2(T,t_1)\right)^{1/2} \quad (12)$$

Thus the position of the ion depends on the pulse duration T and the evolution interval t_1. Only if the ratio of the pulse duration T divided by the ion's period $T_k = 1/\omega_k$ is larger than 10, i.e., when $T/T_k > 10$, can the last term of Eq. 5b be neglected, thereby giving the distance from the centre of the cell, in agreement with the expression given by Guan and Jones.[25]

$$|\vec{R}| \propto \{2(1+\cos[\omega(T-t_{1)}]\}^{1/2} \quad (13)$$

d) Fragmentation interval

The trajectories during the fragmentation interval τ_m can be calculated as before:

$$v_{kx4} = \frac{Eq_k}{4m_k\omega_k}\{\cos[\omega_k(2T+t_1+\tau_m)] - \cos[\omega_k(t_1+\tau_m)] - \cos[\omega_k(T-\tau_m)] + 2\omega_k T\{\sin[\omega_k(2T+t_1+\tau_m)] + \sin[\omega_k(T+\tau_m)]\}\} \quad (14a)$$

$$x_{k4} = \frac{Eq_k}{4m_k\omega_k^2}\{\sin[\omega_k(2T+t_1+\tau_m)] + \sin[\omega_k(T-\tau_m)] - \sin[\omega_k(T+\tau_m)] - \sin[\omega_k(t_1+\tau_m)] - 2\omega_k T\{\cos[\omega_k(2T+t_1+\tau_m)] + \cos[\omega_k(T+\tau_m)]\}\} \quad (14b)$$

$$v_{ky4} = \frac{Eq_k}{4m_k\omega_k}\{\sin[\omega_k(t_1+\tau_m)] - \sin[\omega_k(T-\tau_m)] - \sin[\omega_k(T+\tau_m)] - \sin[\omega_k(2T+t_1+\tau_m)] + 2\omega_k T\{\cos[\omega_k(2T+t_1+\tau_m)] + \cos[\omega_k(T+\tau_m)]\}\} \quad (15a)$$

$$y_{k4} = \frac{Eq_k}{4m_k\omega_k^2}\{8\cos(\omega_k T) - \cos[\omega_k(t_1+\tau_m)] - \cos[\omega_k(T-\tau_m)] + \cos[\omega_k(2T+t_1+\tau_m)] + \cos[\omega_k(T+\tau_m)] + 2\omega_k T\{\sin[\omega_k(2T+t_1+\tau_m)] + \sin[\omega_k(T+\tau_m)]\} - 8\} \quad (15b)$$

Trajectory mapping

The *x* and *y* coordinates calculated above describe the trajectory of the k^{th} ion with a cyclotron frequency ω_k during the entire course of the experiment. In a 2D experiment, the ion acquires a phase $\varphi = \omega_k t_1$ at the end of the evolution interval t_1. Our simulations show trajectories of ions with phases varying in the interval as $0 < \varphi < 2\pi$. We mapped the trajectories for 'matched' pulses where the pulse length matches the precession of the parent ion I^k with frequency ω_k, so that $\omega_k T_1 = \omega_k T_2 = 2\pi n$ with integer n = 1, 2,... The trajectories for n = 1 are shown in Figure 4 for a doubly charged ion of substance P. The case of matched pulses has been discussed previously in the literature.[25,29] When the phase $\omega_k t_1$ acquired by the ion at the end of the evolution interval t_1 is a multiple of 2π, both pulses contribute to excite the ion onto a trajectory with a large radius. If the phase at the end of t_1 is an odd multiple of π, i.e., if $\omega_k t_1 = (2k+1)\pi$, the ion is 'de-excited' back to the centre of the ICR cell by the second pulse.

For 'non-matched' pulses ($\omega_k T_1 = \omega_k T_2 \neq 2\pi n$), the pulse durations $T_1 = T_2$ do not match the precession period. We considered the case where $\omega_k T_1 = \omega_k T_2 < 2\pi$ (Figure 5). Only when the excitation pulse is matched does the ion travel through an integer number of complete circles about the centre of the cell in the interval t_1, so that the trajectories remain centred. For non-matched pulses, the ion's trajectory is no longer centred in the middle of the cell after the excitation pulse. The displacement of the centre of ion's trajectory from the centre of the cell is given by $\vec{d}_{t1}$:

$$\vec{d}_{t1} = \frac{E_0 q_k}{m_k \omega_k^2}\{1 - \cos(\omega_k T)\}\hat{j} \qquad (16)$$

At the end of the encoding sequence, i.e., at the beginning of the fragmentation interval τ_m, the displacement of the centre of the ion's trajectory is exacerbated if the pulses are not matched, pulled in the direction of the applied electric field. The ion orbits in contracting or enlarging circles, with a centre shifted from the centre of the cell, as described by Eq. 17, which is twice the displacement with respect to the centre of the cell during the evolution period.

$$\vec{d}_{\tau m} = \frac{2E_0 q_k}{m_k \omega_k^2}\{1 - \cos(\omega_k T)\}\hat{j} \qquad (17)$$

The actual position of the ion with respect to the centre of the cell, $\vec{\boldsymbol{R}}$, is the vector sum of the displacement of the centre of the ion's orbit, $\vec{\boldsymbol{d}}$, and the position of the ion with respect to the centre of the shifted orbit, $\vec{\boldsymbol{r}}$. The variation of the distance of the ion from the centre of the cell during the fragmentation period $\vec{\boldsymbol{R}}_{\tau m} = \vec{d}_{\tau m} + \vec{r}_{\tau m}$ is shown in Figure 5. For matched pulses, i.e., when $\vec{d}_{\tau m} = 0$, the variation of the distance observed for phases $\pi < \varphi = \omega_k t_1 < 2\pi$ mirrors the variation for $0 < \varphi = \omega_k t_1 < \pi$. But in the case of shifted trajectories, the ions never come back to the centre of the ICR cell during the fragmentation interval τ_m. The ions do however pass periodically near the centre of the cell, depending on the phase $\varphi = \omega_k t_1$ that is acquired at the end of the evolution period. On our FT-ICR spectrometer, the *rf* frequencies during the steps ΔT within the chirp pulses do not correspond exactly to the frequencies of the ions, so that ions excited by a chirp pulse do not experience ideal matched excitation. Thus for most of the ions, the trajectories will be displaced.

The ion is required to be near the centre of the cell for fragmentation by cell-centred techniques to be effective. For pulses that are matched in frequency, the ion returns to the centre of the cell, provided the evolution interval is such that the ion acquires a phase $\varphi = \omega_k t_1 = \pi$. For non-matched pulses, as shown in Figure 6, the ions do not return to the centre of the cell and the efficiency of fragmentation will depend on the overlap of the fragmenting beam with the shifted trajectories of the ions. For example, the laser beam of IRMPD technique exhibits a Gaussian profile at the centre of the ICR cell and the fragmentation thus will not be performed with maximum yield, if the ion's trajectory is not within the breadth of the beam.

The displacements of the ICR orbit with respect to the centre of the cell is very similar to so-called ion-locking experiments, where the centre of an ion's motion is deliberately displaced and the radius of an ion's orbit is increased or decreased by

applying phase shifts of the *rf* fields.[30,31] The shifts that are observed due to a non-matched encoding sequence can be utilized to develop 2D ion-locking experiments based on similar principles as 1D ion-locking experiments. Thus the lack of ions that can be fragmented because they are shifted far away from the centre of the cell can be manipulated to advantage by selectively sequestering the ions and observing them with other combinations of pulses.

Conclusions

When optimizing pulse sequences using frequency-swept 'chirp' pulses, the best results were obtained when using the smallest possible duration for each frequency step (ΔT = 0.5 µs, as opposed to 20 µs for standard excitation pulses). We initially believed that the phase difference $\varphi = \omega_k t_1$ between the ion and the second pulse varies only with the cyclotron frequency ω_k and t_1, so that if the ions would be in-phase with the second pulse P_2, they would be propelled onto a higher radius, whereas if the ion is out-of-phase with respect to P_2, it would be brought back to the centre of the cell.[24] However, this only occurs when the ions are excited by pulses which have *rf* frequencies that are exactly matched with the cyclotron frequency of the ion. We simulated the ion trajectories leading as far as the fragmentation interval τ_m by solving equations of ion movements in an ideal cell. For monochromatic pulses that are on-resonance with the ion's frequency, we observed that during the first pulse the ion gains in kinetic energy, moving in spirals away from the centre. The movement of the ion during the subsequent evolution interval t_1 follows an orbit which is off-centre, unless the product $T_1\omega_k$ of the duration T_1 of the initial excitation pulse and the frequency ω_k of the ion I_k is exactly a multiple of 2π. Hence, the second pulse P_2, even when it is perfectly out-of-phase with respect to the ion, fails to bring the ion back exactly to the centre of the cell, which is essential for performing fragmentation by IRMPD and other cell-centred techniques. In this study, we analysed the motions of ions in the ICR cell in the course of the three-pulse scheme of 2D FT-ICR. By mapping the ion trajectories, we found that the centre of the trajectories of the ions exhibit a displacement with respect to the centre of the cell that varies periodically with the durations of the first two pulses. The shift of the centre leads to off-centred trajectories of the ions during the fragmentation period. These shifted trajectories may lead to a loss in efficiency of cell-centred fragmentation techniques. However, if the pulses are of short duration, the overlap of the laser beam and the precursor ions is not compromised. Another advantage of using pulses of short duration is the decrease of intensities of harmonic signals that appear at multiples of the basic frequencies. Pulses with small durations thus offer a simple way to improve 2D ICR spectra without requiring any sophisticated 'de-noising' techniques.

Acknowledgements

The authors thank the *Centre National de la Recherche Scientifique* (CNRS, France), the *Défi Instrumention aux limites*, the *Agence Nationale pour la Recherche* (ANR, France) (grant 2010FT-ICR2D and grant *Défi de tous les savoirs* 2014, ONE_SHOT_FT-ICR_MS_2D) and the European Research Council (ERC, advanced grant 'Dilute para water') for financial support.

Appendix

Glossary for ICR adapted from the work of van Agthoven et al[32]

Encoding sequence: The sequence which encodes the frequencies of the precursor ions prior to fragmentation which is normally composed of an 'excitation' pulse, an evolution interval, and an 'encoding' pulse.

Excitation pulse: First pulse (designated by P_1) of the pulse sequence, which excites all precursor ions equally.

Evolution interval (previously referred to as frequency encoding period): Regularly incremented interval, designated as t_1, between the two pulses of the encoding sequence, during which all precursor ions rotate at their cyclotron frequency.

Encoding pulse: Second pulse (designated by P_2) of the pulse sequence, which modifies the radius of the trajectories depending on the phase of the ions.

Fragmentation period: Fixed interval between the encoding pulse and the detection pulse during which precursor ions are fragmented.

Detection pulse (previously referred as observe pulse): Third pulse (designated as P_3) of the pulse sequence, which excites both precursor and fragment ions prior to detection.

References

1 I. Noda, *J. Am. Chem. Soc.*, 1989, **111**, 8116–8118.

2 J. Gorcester and J. H. Freed, *J. Chem. Phys.*, 1988, **88**, 4678–4693.

3 P. Pfandler, G. Bodenhausen, J. Rapin, R. Houriet and T. Gaumann, *Chem. Phys. Lett.*, 1987, **138**, 195–200.

4 J. D. Hybl, A. A. Ferro and D. M. Jonas, *J. Chem. Phys.*, 2001, **115**, 6606–6622.

5 D. M. Jonas, *Annu. Rev. Phys. Chem.*, 2003, **54**, 425–463.

6 W. P. Aue, E. Bartholdi and R. R. Ernst, *J. Chem. Phys.*, 1976, **64**, 2229–2246.

7 A. G. Marshall, *Acc. Chem. Res.*, 1996, **29**, 307–316.

8 A. G. Marshall and T. Chen, *Int. J. Mass Spectrom.*, 2015, **377**, 410–420.

9 E. L. Hahn, *Phys. Rev.*, 1950, **80**, 580–594.

10 H. Oschkinat, A. Pastore and G. Bodenhausen, *J. Am. Chem. Soc.*, 1987, **109**, 4110–4111.

11 H. Oschkinat, D. Limat, L. Emsley and G. Bodenhausen, *J. Magn. Reson.*, 1989, **81**, 13–42.

12 H. Oschkinat, A. Pastore, P. Pfändler and G. Bodenhausen, *J. Magn. Reson.*, 1986, **69**, 559–566.

13 M. J. Thrippleton and J. Keeler, *Angew. Chemie - Int. Ed.*, 2003, **42**, 3938–3941.

14 G. Bodenhausen, H. Kogler and R. R. Ernst, *J. Magn. Reson.*, 1984, **58**, 370–388.

15 R. A. Zubarev, N. L. Kelleher and F. W. Mclafferty, *J. Am. Chem. Soc.*, 1998, **120**, 3265–3266.

16 B. A. Budnik, K. F. Haselmann and R. A. Zubarev, *Chem. Phys. Lett.*, 2001, **342**, 299–302.

17 P. Hvelplund, B. Liu, S. B. Nielsen and S. Tomita, *Int. J. Mass Spectrom.*, 2003, **225**, 83–87.

18 J. E. P. Syka, J. J. Coon, M. J. Schroeder, J. Shabanowitz and D. F. Hunt, *Proc. Natl. Acad. Sci. U. S. A.*, 2004, **101**, 9528–33.

19 D. P. Little, J. P. Speir, M. W. Senko, P. B. O'Connor and F. W. McLafferty, *Anal. Chem.*, 1994, **66**, 2809–15.

20 P. D. Schnier, W. D. Price, R. A. Jockusch and E. R. Williams, *J. Am. Chem. Soc.*, 1996, **118**, 7178–7189.

21 J. M. Wells and S. A. McLuckey, *Methods Enzymol.*, 2005, **402**, 148–85.

22 G. Baykut and J. R. Eyler, *Trends Anal. Chem.*, 1986, **5**, 44–49.

23 L. Chen and A. G. Marshall, *Int. J. Mass Spectrom. Ion Process.*, 1987, **79**, 115–125.

24 A. G. Marshall and D. C. Roe, *J. Chem. Phys.*, 1980, **73**, 1581.

25 S. Guan and P. R. Jones, *J. Chem. Phys.*, 1989, **91**, 5291–5295.

26 M. A. Van Agthoven, L. Chiron, M. A. Coutouly, A. A. Sehgal, P. Pelupessy, G. Bodenhausen, M. Delsuc and C. Rolando, *Int. J. Mass Spectrom.*, 2014, **370**, 114–124.

27 L. Chiron, M. A. Van Agthoven, B. Kieffer, C. Rolando and M.-A. Delsuc, *Proc. Natl. Acad. Sci. U. S. A.*, 2014, **111**, 1385–90.

28 S.-P. Chen and M. B. Comisarow, *Rapid Commun. Mass Spectrom.*, 1991, **5**, 450–455.

29 A. G. Marshall, T.-C. L. Wang and T. L. Ricca, *Chem. Phys. Lett.*, 1984, **105**, 233–236.

30 C. Ruidan, A. G. Marshall and M. Wang, *Chem. Phys. Lett.*, 1991, **18**, 168–174.

31 R. T. Mciver, *Int. J. Mass Spectrom. Ion Process.*, 1989, **89**, 343–358.

32 M. A. Van Agthoven, M.-A. Delsuc, G. Bodenhausen and C. Rolando, *Anal. Bioanal. Chem.*, 2013, **405**, 51–61.

Figure Legend

Figure 1. (a) Sequence for 2D exchange spectroscopy (EXSY) with a notation commonly used in NMR, i.e.: $\beta - t_1 - \beta' - \tau_m - \beta'' - t_2$ with nutation angles (or 'flip angles') β, β' and β''. (b) 2D FT-ICR sequence $P_1 - t_1 - P_2 - \tau_m - P_3 - t_2$ with three pulses P_1, P_2 and P_3 of lengths T_1, T_2 and T_3.

Figure 2. (a) Detailed view of a 2D ICR sequence where the time axis is sequentially labelled 1, 2, etc. to distinguish the beginning and end of various intervals. (b) 2D ICR spectrum for a vanishingly short fragmentation interval $\tau_m = 0$. The signals evolve with the same frequency in both t_1 and t_2 intervals, so that one only sees a single diagonal peak, $\omega_1 = \omega_2 = \Omega^k$. (c) If some of the ions break up during the fragmentation interval τ_m, the parent signals appear at $\omega_1 = \Omega^k$ and the signals of the fragments or daughter ions at $\omega_2 = \Omega^l$, in this example with $\Omega^l > \Omega^k$.

Figure 3. Encoding sequence of the 2D ICR scheme showing the first two chirp pulses. For the sake of illustration, the pulse is broken down into blocks corresponding to frequencies stepped from ω_i to ω_f. The black block represents the frequency ω_k corresponding to the k^{th} ion.

Figure 4. Trajectories for matched pulses with durations T so that $\omega_k T = 2\pi$. The ion's frequency is ω_k = 200 kHz, corresponding to the doubly charged ion of substance P in a field of 8.78 T, the evolution interval is taken to be t_1 = 10 μs, the excitation and encoding pulses have durations $T_1 = T_2$ = 5 μs and the pulse voltage is 2666 V, which is proportional to the default pulse voltage. The pulse area remains constant. Blue bullets represent the ions, red bullets the centre of the trajectories during the evolution and fragmentation intervals.

Figure 5. Trajectories for short excitation and encoding pulses with durations so that $\omega_k T_1 = \omega_k T_2 < 2\pi$. The excitation and encoding pulses have durations $T_1 = T_2$ = 4 μs. The remaining conditions are same as in Figure. 4. Blue bullets represent the ions, red bullets the centres of the trajectories during the evolution interval, and black bullets the centres of the trajectories during the fragmentation interval.

Figure 6. Variation of the distance of ions with respect to the centre of the cell during the fragmentation interval (a) for matched pulses, (b) for non-matched pulses. The colour code represents the phase $\varphi = \omega_k t_1$ that the ions acquire at the end of the evolution interval. The bottom and top figure indicates the variation for phase change from 0 to π and π to 2π respectively.

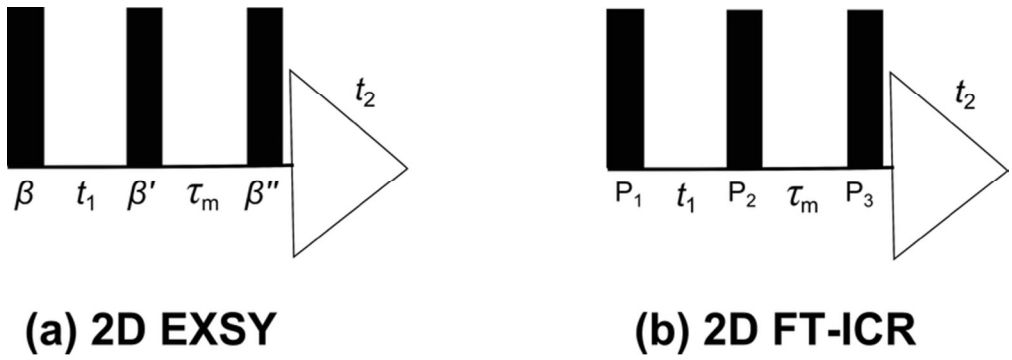

(a) 2D EXSY **(b) 2D FT-ICR**

Figure 1. (a) Sequence for 2D exchange spectroscopy (EXSY) with a notation commonly used in NMR, i.e.: $\beta - t_1 - \beta' - \tau_m - \beta'' - t_2$ with nutation angles (or 'flip angles') β, β' and β''. (b) 2D FT-ICR sequence $P_1 - t_1 - P_2 - \tau_m - P_3 - t_2$ with three pulses P_1, P_2 and P_3 of lengths T_1, T_2 and T_3.
71x24mm (300 x 300 DPI)

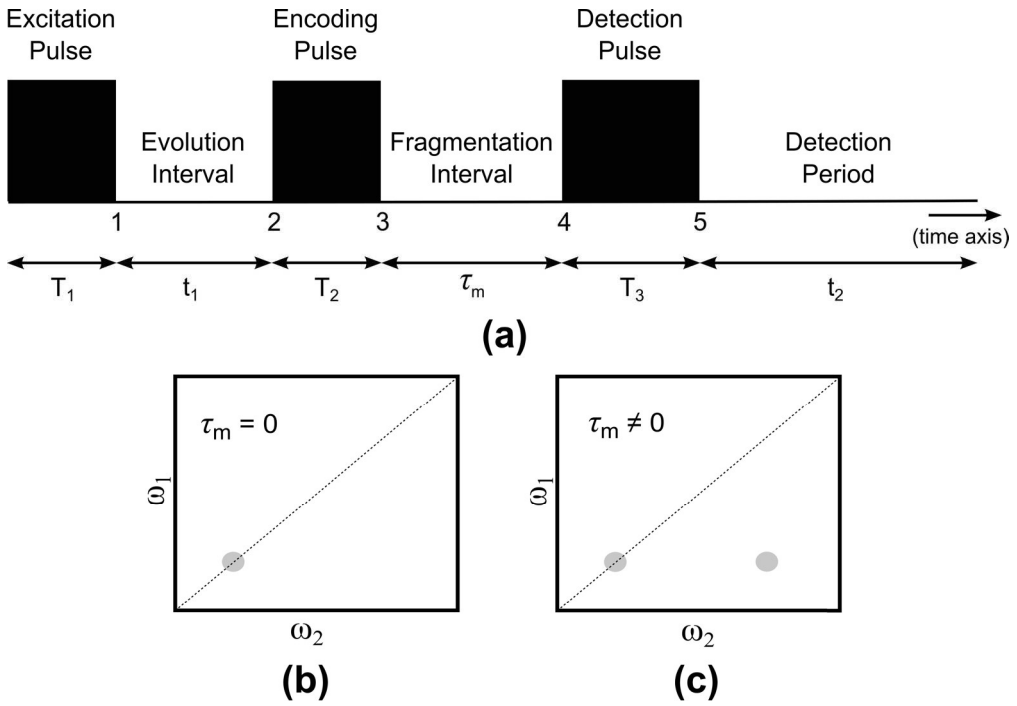

Figure 2. (a) Detailed view of a 2D ICR sequence where the time axis is sequentially labelled 1, 2, etc. to distinguish the beginning and end of various intervals. (b) 2D ICR spectrum for a vanishingly short fragmentation interval $\tau_m = 0$. The signals evolve with the same frequency in both t_1 and t_2 intervals, so that one only sees a single diagonal peak, $\omega_1 = \omega_2 = \Omega^k$. (c) If some of the ions break up during the fragmentation interval τ_m, the parent signals appear at $\omega_1 = \Omega^k$ and the signals of the fragments or daughter ions at $\omega_2 = \Omega^l$, in this example with $\Omega^l > \Omega^k$.
185x127mm (300 x 300 DPI)

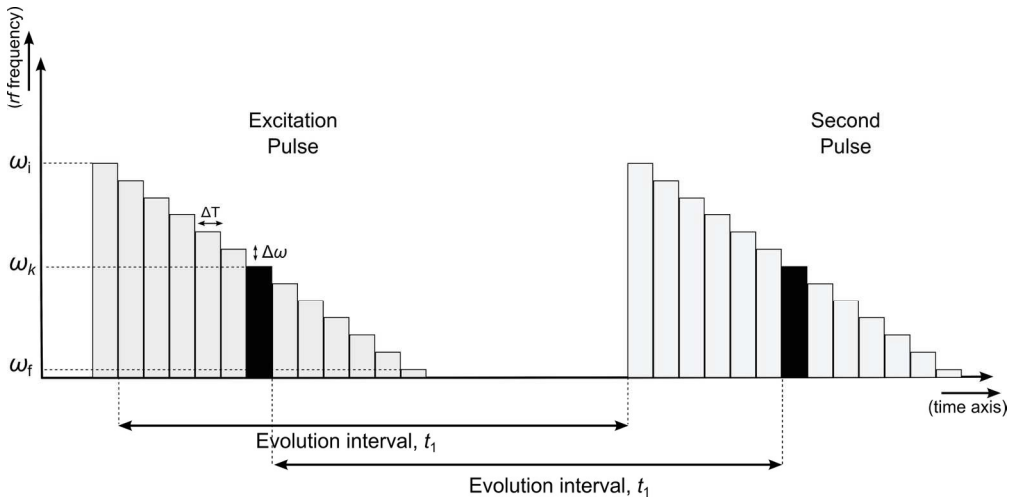

Figure 3. Encoding sequence of the 2D ICR scheme showing the first two chirp pulses. For the sake of illustration, the pulse is broken down into blocks corresponding to frequencies stepped from ω_i to ω_f. The black block represents the frequency ω_k corresponding to the k^{th} ion.
160x78mm (300 x 300 DPI)

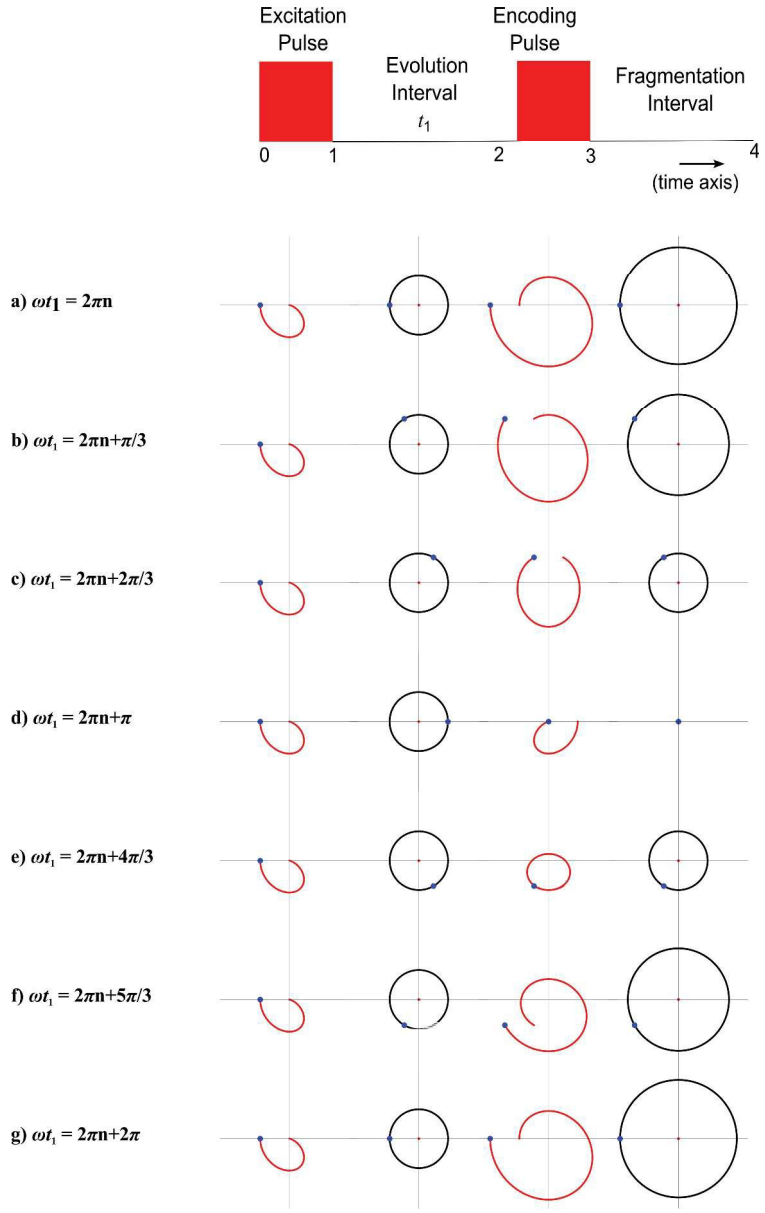

Figure 4. Trajectories for matched pulses with durations T so that $\omega_k T = 2\pi$. The ion's frequency is ω_k = 200 kHz, corresponding to the doubly charged ion of substance P in a field of 8.78 T, the evolution interval is taken to be t_1 = 10 μs, the excitation and encoding pulses have durations $T_1 = T_2$ = 5 μs and the pulse voltage is 2666 V, which is proportional to the default pulse voltage. The pulse area remains constant. Blue bullets represent the ions, red bullets the centre of the trajectories during the evolution and fragmentation intervals.
487x783mm (300 x 300 DPI)

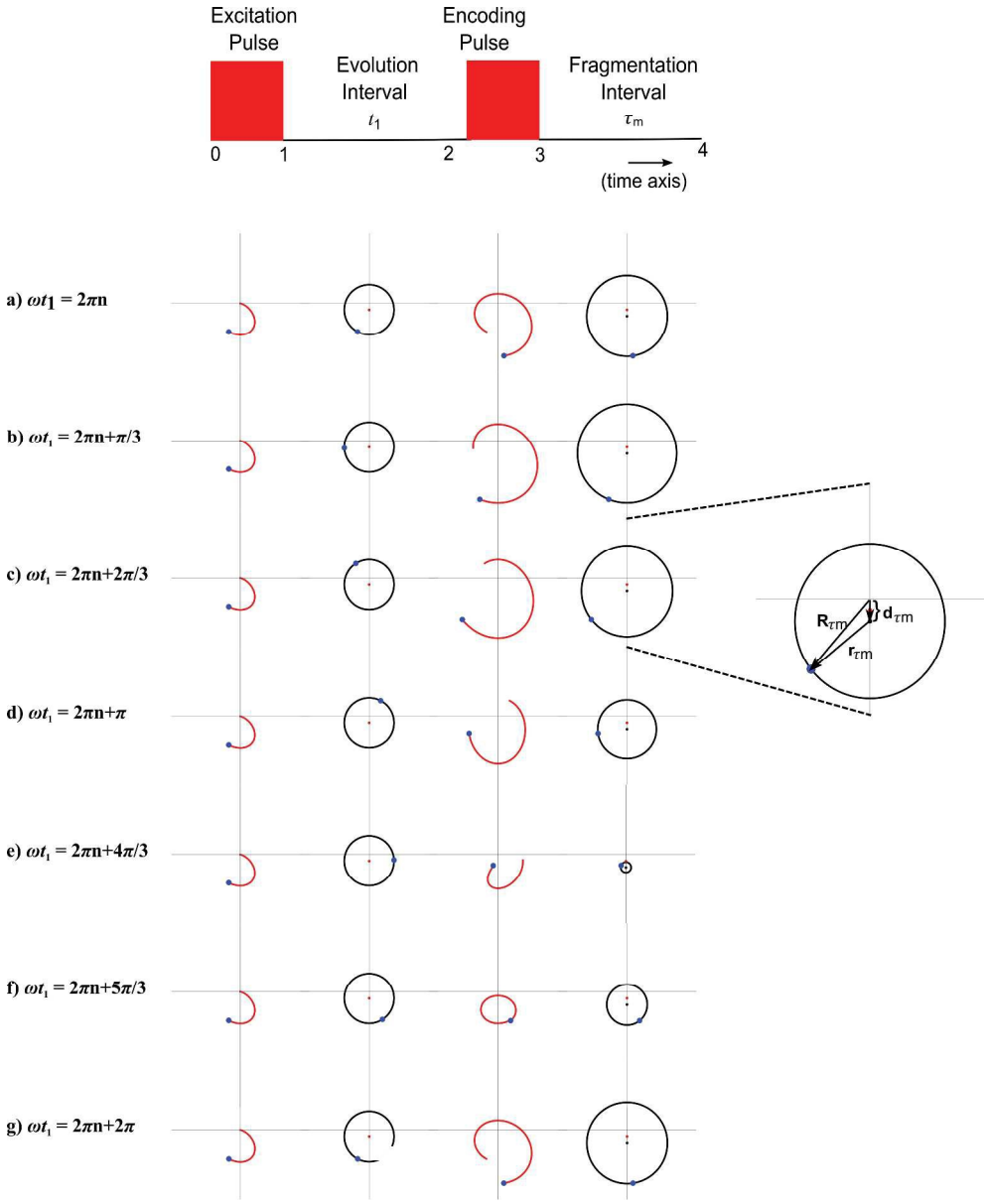

Figure 5. Trajectories for short excitation and encoding pulses with durations so that $\omega_k T_1 = \omega_k T_2 < 2\pi$. The excitation and encoding pulses have durations $T_1 = T_2 = 4$ μs. The remaining conditions are same as in Figure. 4. Blue bullets represent the ions, red bullets the centres of the trajectories during the evolution interval, and black bullets the centres of the trajectories during the fragmentation interval.
487x595mm (300 x 300 DPI)

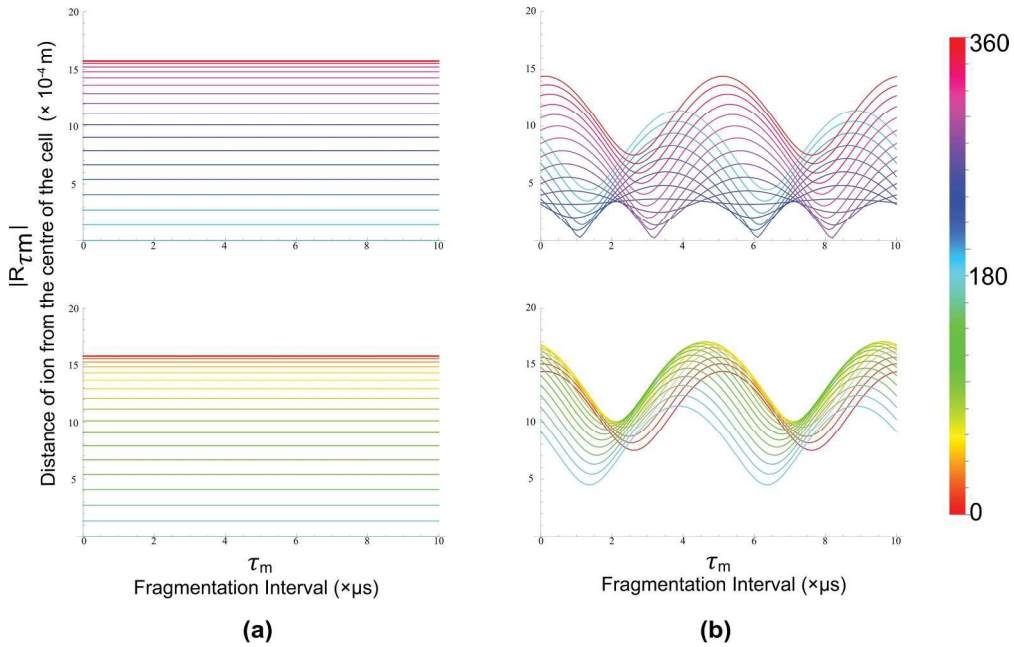

Figure 6. Variation of the distance of ions with respect to the centre of the cell during the fragmentation interval (a) for matched pulses, (b) for non-matched pulses. The colour code represents the phase $\varphi = \omega_k t_1$ that the ions acquire at the end of the evolution interval. The bottom and top figure indicates the variation for phase change from 0 to π and π to 2π respectively.
207x131mm (300 x 300 DPI)